



Investigation of subgrid-scale mixing of reactive scalar perturbations from flamelets in turbulent partially premixed flames



Shuaishuai Liu, Chenning Tong*

Department of Mechanical Engineering, Clemson University, Clemson, SC 29634, United States

ARTICLE INFO

Article history:

Received 22 April 2015

Revised 23 July 2015

Accepted 25 July 2015

Available online 4 September 2015

Keywords:

Turbulent flames

Flamelet

Large-eddy simulation

Filtered density function

Turbulent mixing

ABSTRACT

Recent studies of subgrid-scale (SGS) mixing and turbulence-chemistry interaction have shown that turbulent flames contain different structures. In flamelet structures diffusion of reactive scalars and chemical reaction are tightly coupled. Most mixing models used in probability density and filtered density methods, however, are based on non-reactive scalars. To investigate the effects of the coupling on the diffusion we decompose a reactive scalar into a steady flamelet part and perturbations from it. The diffusion of the former can be obtained from a suitably chosen flamelet solution while the latter is unclosed. The conditionally filtered diffusion and dissipation of the reactive scalar perturbations are analyzed using high-resolution line images obtained in turbulent partially premixed (Sandia) flames. For SGS scalar containing flamelets, the perturbation diffusion has characteristics similar to that of a non-reactive scalar, in contrast with the flamelet part. The functional form of the conditionally filtered diffusion is well described by the Interaction by Exchange with the Mean (IEM) model. Our perturbation analysis of the flamelet equation shows that for perturbations having length scales smaller than the reaction zone width, the reactive scalar diffusion is largely controlled by the mixture fraction field, thus having the characteristics of non-reactive scalar mixing. For perturbations with length scales larger than the reaction width, the conditionally filtered diffusion has the same form as non-reactive scalar mixing, with the mixing time scale determined by the flamelet. The IEM model predictions based on this mixing time scale are in good agreement with the experimental results for a range of SGS conditions, suggesting that the perturbations are consistent with unsteady flamelets for the conditions studied. Thus, mixing models based on non-reactive scalars can potentially model the SGS mixing accurately. The results in the present study can be useful for developing a unified mixing model that can predict all combustion regimes accurately.

© 2015 The Combustion Institute. Published by Elsevier Inc. All rights reserved.

1. Introduction

Turbulent flames contain a wide range of length scales as well as structures, which presents a great modeling challenge. Two important and distinct categories of turbulent combustion models are probability density function (PDF) like and flamelet-like [1]. Models in each category are advantageous in predicting different flame structures. Flamelet models are more accurate for predicting flamelet combustion while PDF models in principle can model all flame structures. Current mixing models used in PDF models, however, generally are based on turbulence-controlled mixing, and therefore may be more accurate for non-reactive scalars and distributed reaction zones, and are expected to be less accurate for flamelets, because mixing (diffusion) of reactive scalars in them is enhanced by reaction.

Several approaches have been proposed to improve predictions of flamelet combustion by PDF models. Haworth et al. [2] proposed an approach for partially premixed combustion employing the PDF method for a reduced set of variables (e.g. mixture fraction) combined with a flamelet library. Pope [3] proposed a hybrid approach to explicitly include the flamelet structure into the PDF formalism, combining the chemical source term and the mixing term. The combined term is a unique function of the reaction progress variable in a premixed laminar flamelet. In this approach the tight coupling between mixing and reaction in flamelets is accounted for using a flamelet library and no longer needs modeling.

Turbulent flames, especially at high Reynolds numbers, however, can contain a range of structures, including flamelets and distributed reaction zones. Even when flamelets are the dominant flame structure, there can be significant deviations from them, which mixing models need to account for. In the present study we investigate reactive scalar mixing in turbulent partially premixed flames to understand the extent of coupling between mixing and reaction when

* Corresponding author. Tel.: +01 864 6567225; Fax: +864 6564435.
E-mail address: ctong@clemson.edu (C. Tong).

perturbations from flamelets exist, and how mixing may be modeled more accurately. We study perturbations from flamelets burning in non-premixed mode. While under certain conditions premixed-mode burning can occur in partially premixed flames, the fuel stream composition of the Sandia flames supports only flamelets in non-premixed mode.

Since the diffusion in flamelets is strongly coupled to reaction, the degree of coupling of the perturbation diffusion to the reaction term is of interest. We decompose a reactive scalar, say temperature T , into a steady flamelet part, $T^f(Z, \chi_s^f)$, and perturbations from it, T^* , where Z , χ_s^f , and T^f are mixture fraction, the stoichiometric mixture fraction dissipation rate, and a steady flamelet solution, respectively. Following Bilger [4] and Peters [5] the transport equation of T can be written as

$$\begin{aligned} \rho \frac{\partial T^*}{\partial t} + \rho \frac{\partial T^f}{\partial Z} \frac{\partial Z}{\partial t} + \rho u_k \frac{\partial T^*}{\partial x_k} + \rho u_k \frac{\partial Z}{\partial x_k} \frac{\partial T^f}{\partial Z} \\ = \frac{\partial}{\partial x_k} \left(\rho D \frac{\partial T^*}{\partial x_k} \right) + \frac{\partial}{\partial x_k} \left(\rho D \frac{\partial T^f}{\partial x_k} \right) + w_T \\ = \frac{\partial}{\partial x_k} \left(\rho D \frac{\partial T^*}{\partial x_k} \right) + \frac{\partial}{\partial x_k} \left(\rho D \frac{\partial Z}{\partial x_k} \right) \frac{\partial T^f}{\partial Z} + \rho \frac{\chi}{2} \frac{\partial^2 T^f}{\partial Z^2} + w_T, \quad (1) \end{aligned}$$

where D , u_k , and w_T are diffusivity, velocity component, and chemical source term, respectively. The third term on the second line of Eq. (1) represents the diffusion of T induced by reaction, reflecting the coupling between mixing and reaction. For a suitably defined diffusivity, the terms containing $\frac{\partial T^f}{\partial Z}$ sum to zero, resulting in the transport equation for T^*

$$\rho \frac{\partial T^*}{\partial t} + \rho u_k \frac{\partial T^*}{\partial x_k} = \frac{\partial}{\partial x_k} \left(\rho D \frac{\partial T^*}{\partial x_k} \right) + \rho \frac{\chi}{2} \frac{\partial^2 T^f}{\partial Z^2} + w_T. \quad (2)$$

The second term on the RHS can also be interpreted as the production (or generation) of T^* due to mixing. When the perturbations are not very large (e.g., with T above local extinction values), this term and w_T are the dominant terms, balancing each other exactly when $T^* = 0$, i.e., in a steady flamelet. Thus, the diffusion of T^* depends on the deviations of χ from the flamelet values. It is therefore likely that some temperature perturbations may not have the structure of the flamelets. If it is possible to model the diffusion of T^* using mixing models based on non-reactive scalars, an indirect model for the diffusion of T can be obtained from the first three terms on the RHS of Eq. (1).

In the context of the PDF methods, the mixing process that evolves the mass density function (MDF), F_{ZT} , of Z and T , can be studied using the unclosed mixing terms in the MDF transport equation [6], the conditional mixture fraction diffusion and temperature diffusion, $\langle \frac{1}{\rho} \frac{\partial}{\partial x_i} (\rho D \frac{\partial Z}{\partial x_i}) | Z = \hat{Z}, T = \hat{T} \rangle$, $\langle \frac{1}{\rho} \frac{\partial}{\partial x_i} (\rho D \frac{\partial T}{\partial x_i}) | Z = \hat{Z}, T = \hat{T} \rangle$, or alternatively, the conditional mixture fraction dissipation, temperature dissipation, and the cross dissipation, $\langle \chi | Z = \hat{Z}, T = \hat{T} \rangle \equiv \langle 2D \frac{\partial Z}{\partial x_i} \frac{\partial Z}{\partial x_i} | Z = \hat{Z}, T = \hat{T} \rangle$, $\langle \chi_T | Z = \hat{Z}, T = \hat{T} \rangle \equiv \langle 2D \frac{\partial T}{\partial x_i} \frac{\partial T}{\partial x_i} | Z = \hat{Z}, T = \hat{T} \rangle$, $\langle \chi_{ZT} | Z = \hat{Z}, T = \hat{T} \rangle \equiv \langle 2D \frac{\partial Z}{\partial x_i} \frac{\partial T}{\partial x_i} | Z = \hat{Z}, T = \hat{T} \rangle$, respectively, where \hat{Z} and \hat{T} are the sample-space variables for Z and T , respectively, and are omitted hereafter for convenience. The angle brackets denote ensemble averages. To investigate the extent of the coupling between mixing and reaction, the conditional diffusion of the reactive scalar (e.g., temperature) can be decomposed into two terms:

$$\begin{aligned} \left\langle \frac{1}{\rho} \frac{\partial}{\partial x_i} \left(\rho D \frac{\partial T}{\partial x_i} \right) \middle| Z, T \right\rangle \\ = \left\langle \frac{1}{\rho} \frac{\partial}{\partial x_i} \left(\rho D \frac{\partial T^f}{\partial x_i} \right) \middle| Z, T \right\rangle + \left\langle \frac{1}{\rho} \frac{\partial}{\partial x_i} \left(\rho D \frac{\partial T^*}{\partial x_i} \right) \middle| Z, T \right\rangle. \quad (3) \end{aligned}$$

The conditional dissipation rate can be decomposed into three terms:

$$\begin{aligned} \chi_T &\equiv \left\langle 2D \frac{\partial T}{\partial x_i} \frac{\partial T}{\partial x_i} \middle| Z, T \right\rangle \\ &= \left\langle 2D \frac{\partial T^f}{\partial x_i} \frac{\partial T^f}{\partial x_i} \middle| Z, T \right\rangle + \left\langle 2D \frac{\partial T^*}{\partial x_i} \frac{\partial T^*}{\partial x_i} \middle| Z, T \right\rangle \\ &\quad + \left\langle 4D \frac{\partial T^f}{\partial x_i} \frac{\partial T^*}{\partial x_i} \middle| Z, T \right\rangle. \quad (4) \end{aligned}$$

With flamelet solutions, the first terms on the RHS of Eqs. (3) and (4) contain the scalar (mixture fraction) dissipation rate (see Eqs. (6) and (8)) and do not require modeling of reaction scalar mixing. The dissipation and diffusion of the temperature perturbations still require modeling.

To analyze the diffusion of reactive scalar perturbations from steady flamelet solutions using experimental data, we apply the conditional sampling method we developed previously [7–9] to select instantaneous local flame regions that contain flamelets. Our previous studies of subgrid-scale (SGS) mixing in the context of large-eddy simulation of turbulent combustion [7–12] have shown that local regions containing flamelets can be selected by conditioning on the SGS scalar variance. The SGS scalar at a fixed location has qualitatively different filtered density function (PDF) shapes and structures depending on the instantaneous SGS scalar variance. When the SGS variance is large compared to its mean value, the SGS scalar has bimodal distributions, indicating that the fuel-lean and fuel-rich regions of the SGS fields are highly segregated. There is a ramp-cliff structure separating the two regions, across which there is a large scalar value jump, resulting in a conditional SGS structure resembling that of a counter-flow non-premixed flame, which is a model for laminar flamelets. Thus, we can use large values of the SGS variance to select SGS scalars containing flamelets. We use the Favre filtered mixture fraction, $\langle Z \rangle_L = \langle \rho Z \rangle_\ell / \langle \rho \rangle_\ell$, and the Favre SGS scalar variance,

$$\langle Z'^2 \rangle_L \equiv \frac{1}{\langle \rho \rangle_\ell} \int F_{ZL}(Z; \mathbf{x}, t) (Z - \langle Z \rangle_L)^2 dZ = \langle \rho Z^2 \rangle_\ell / \langle \rho \rangle_\ell - \langle Z \rangle_L^2, \quad (5)$$

as conditioning variables, where $\langle \cdot(\mathbf{x}) \rangle_\ell = \int \cdot(\mathbf{x}') G(\mathbf{x} - \mathbf{x}') d\mathbf{x}'$, and $\langle \cdot(\mathbf{x}) \rangle_L = \frac{1}{\langle \rho \rangle_\ell} \int \cdot(\mathbf{x}') \rho(\mathbf{x}', t) G(\mathbf{x} - \mathbf{x}') d\mathbf{x}'$, denote conventional and Favre filtering with a top-hat filter, respectively. The Favre filtered mixture fraction, $\langle Z \rangle_L$, is set to the stoichiometric mixture fraction, $Z_s (= 0.35)$, to maximize the probability of the SGS fields containing reaction zones. The Favre SGS scalar variance is set to values larger than seven times its mean value to sample the SGS fields containing flamelets.

In the present study we analyze the conditionally filtered diffusion and dissipation of the reactive scalar perturbations from steady flamelet solutions using experimental data obtained in the Sandia flames. Knowledge of the mixing properties of the perturbations is an important step in understanding the coupling effects between molecular transport and chemical reaction in turbulent flames. The results are relevant for improving modeling approaches, including the laminar flamelet and the filtered mass density (FMDf) approaches for large-eddy simulation of turbulent combustion.

2. Experimental data and processing procedures

We use experimental data obtained in piloted turbulent partially premixed methane jet flames with a 1:3 ratio of CH_4 to air by volume (Sandia flames D and E, see [13,14] for details). The Reynolds number of flame D and E are 22,400 and 33,600, respectively. The fuel jet diameter is 7.2 mm. The measurements employed combined line imaging of Raman scattering, Rayleigh scattering, and laser-induced CO fluorescence. Simultaneous measurements of the major species (CO_2 ,

O₂, CO, N₂, CH₄, H₂O, and H₂), the mixture fraction (obtained from all major species), the temperature, and the radial component of scalar dissipation rate were made. In each flame, approximately 6000 line images are available at each measurement location. The mixture fraction is calculated using a variation of Bilger's definition [15], which has been modified by excluding the oxygen terms. The length of the imaging line is 6.0 mm with a pixel spacing of 0.2 mm.

Measurement noise can contribute to the perturbations obtained using experimental data. The typical uncertainty in the Sandia flame data is 1% for the temperature and the major species except the hydrogen mass fraction, Y_{H_2} , which has an uncertainty of 6%. The perturbations obtained in the present study are generally much larger. More important, the conditional scalar dissipation associated with the perturbations is consistent with flame behaviors, with a higher dissipation rate corresponding to a lower temperature and vice versa. Thus, the experimental noise does not qualitatively alter the results obtained in the present study.

The steady flamelet library used in the analysis is for the counterflow configuration generated using the FlameMaster code [16]. The chemistry mechanism is the GRI-Mech 3.0 for methane and air [17], which contains 325 reactions and 53 species. Barlow et al. [18,19] have shown that it predicts the Sandia flame B (a laminar flame) well. In this work, effects of radiation on the major species and temperature are neglected in the flamelet calculations as previous studies have shown that they are quite small in the Sandia flames [20,21].

Calculations of the conditionally filtered variables require spatial filtering of scalar fields. In this work a simple top-hat filter is chosen because it is (i) used in most if not all FDF/LES and (ii) it is positive, thus ensuring that the filtered (fine-grained) density has the property of a density. A spectral filter, however, cannot ensure positiveness of the filtered density. The line images are used to perform one-dimensional filtering. Thus we obtain one component of the filtered variables. For the same filter width one-dimension filter results in a somewhat higher SGS variance than a three-dimensional one, affecting the conditionally filtered scalar diffusion and dissipation. This increase, however, is not sufficiently large to significantly alter the functional forms of the variables. Small-scale anisotropy can also result in differences between the scalar diffusion and dissipation components obtained using one- and three-dimensional data. Given the moderate level of anisotropy in free shear flows, however, we expect the one-dimensional results to be similar to three-dimensional results.

The filter width employed in this work is 3.0 mm, significantly larger than the dissipative (Corrsin) scales (0.065–0.106 mm [22]), so that the subgrid scales contain sufficient fluctuations. This filter width is not very small compared to the integral length scales. Nevertheless, given Reynolds number of the Sandia flames, they are preferable than smaller filter sizes, which will not be much larger than the Corrsin scale. Previous studies (e.g., Refs. [7,9]) have shown that when the filter width is much larger than the dissipation scales the properly scaled conditional statistics are not sensitive to the filter width.

In the present study the dissipation and diffusion terms are calculated using 10th-order explicit central differencing schemes. While the measurement noise affects the conditional mean diffusion obtained from the experimental data, the effects are not amplified by the finite difference scheme because the noises from different samples are uncorrelated and their contributions to the diffusion are canceled when calculating the conditional mean. The noise only enters through the conditioning variable, whose value is the sum of the scalar value and the noise. Thus the measured conditional diffusion is the noise-free diffusion averaged over the PDF of the noise, and therefore depends on the curvature of the conditional diffusion in the scalar sample space (the second derivative). Because significant curvature effects of the conditional mean only occur over large-scale scalar fluctuations, which is much larger than the noise variance, the effects of the noise are negligible.

Previous results [18] as well as our calculations have shown that the Lewis number has strong effects on the laminar flame prediction for the fuel used in the Sandia flames. Barlow et al. [18] have shown that in Sandia flame B, which has a low Reynolds number and is laminar, the measurements are in good agreement with laminar flame calculations with detailed molecular transport (using the Tsuji burner configuration). However, in flame E at $x/d = 45$, the data agree well with the unity Lewis number calculations, where x and d are the distance downstream of the nozzle and the nozzle diameter, respectively. In Fig. 1 we compare the conditionally filtered scalars (e.g., $\langle (T/Z)_L | (Z)_L \rangle$, $\langle (Z'^2)_L \rangle$) at $x/d = 30$ in flame E, where line images are available for calculating diffusion and dissipation, with flamelet calculations using both unity and non-unity Lewis numbers. The measured conditional mean temperature and mass fractions are in good agreement with the unity Lewis number prediction, although not to the same extent as at $x/d = 45$ for Y_{H_2} and Y_{CO_2} . These results suggest that the Lewis number effects in the Sandia flames are quite complex, depending both the Reynolds number and the downstream location. Due to the complexity of the differential diffusion effects in turbulent flames, in the present study we use unity Lewis number in the flamelet calculations and focus on the temperature and Y_{H_2O} at $x/d = 30$ in flame E, because differential diffusion effects for these variables are small at this location, as evidenced by the excellent approximations of their conditional means by the flamelet calculations. In addition, at this location the flame is highly turbulent; therefore the SGS mixing is more representative of high-Reynolds-number turbulent flames. We also use the temperature data at $x/d = 15$ in flame E and $x/d = 15$ and 30 in flame D, which are only weakly affected by differential diffusion. The issue of differential diffusion will be addressed in a future study.

3. Results

In the present study, due to the limited amount of data available, care must be taken to ensure sufficient convergence for the statistics obtained. Thus, we choose only one SGS variance value much larger than the mean SGS variance when sampling the SGS fields containing flamelets so that a relatively large bin size can be used to ensure sufficient number of samples are obtained. We only analyze the burning samples, as our objective is to examine the mixing process in burning flamelets (local extinction and reignition pose different modeling challenges and are beyond the scope of this work). The flamelet solution at $\chi_s^f = 610/s$ (extinction limit) is used to separate the (nominally) extinguished samples from the burning samples, where χ_s^f is scalar dissipation rate at the stoichiometric mixture fraction. The line images containing extinguished samples are excluded. The flamelet solution for which the $Z - T$ and $Z - Y_{H_2O}$ profiles are closest to the conditional means obtained from the burning samples is chosen. Figure 1 shows that for flame E at $x/D = 30$ the flamelet with $\chi_s^f = 143/s$ closely matches the conditional means of the temperature and Y_{H_2O} for the SGS scalar variance chosen. It also better matches the conditional means of Y_{CO_2} , and Y_{H_2} than other values of χ_s^f (not shown).

We choose a steady flamelet solution T^f in our analysis instead of the conditional mean $\langle T|Z \rangle$ for two reasons. First, since the goal is to model diffusion in the flamelet regime more accurately, it is natural to use the flamelet solution and model perturbations from it. Second, a flamelet is a physical model for flame structure and a flamelet solution is an exact solution of the flamelet equation. The conditional mean, however, is a statistic and the solution of its equation involve additional assumptions. In particular, assumptions on the conditional reaction term and the covariance of conditional fluctuations are needed. Thus, the equation for the conditional perturbations is more complex than that for the perturbations from a flamelet, making modeling and asymptotic analyses more difficult. In addition, the functional form of the conditional mean obtained

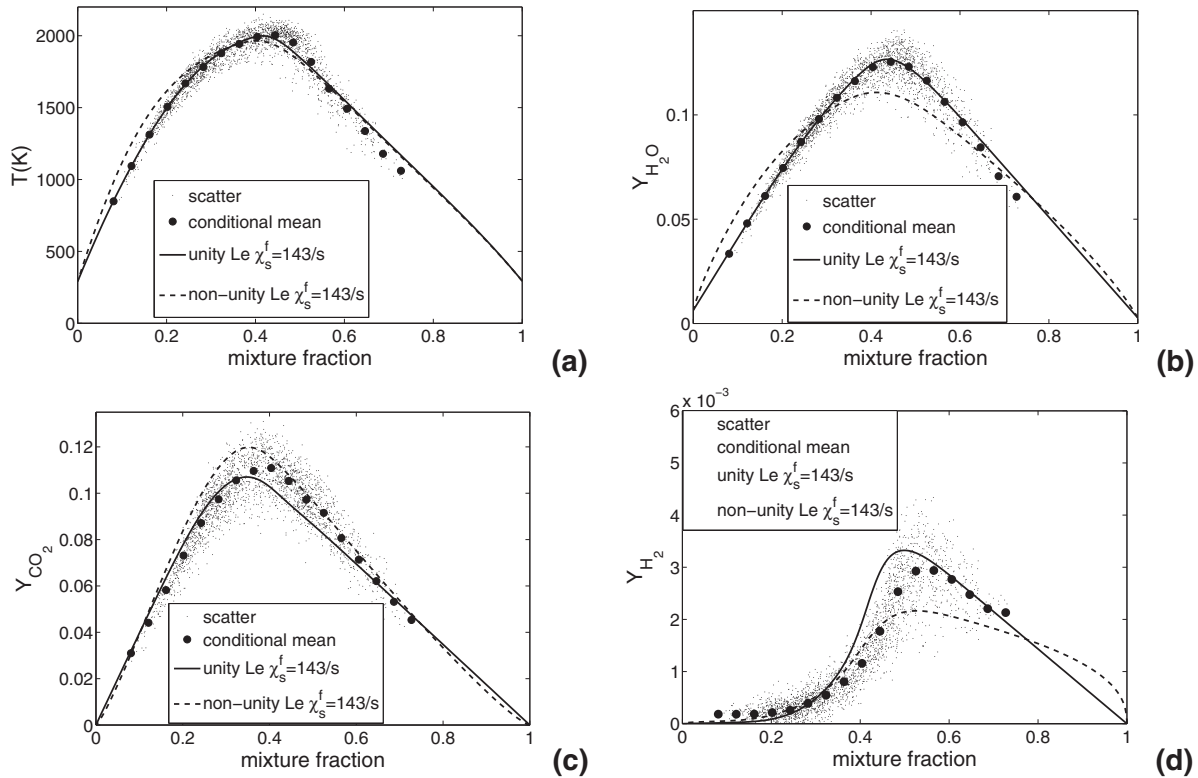


Fig. 1. Measured conditionally filtered mean of (a) temperature and (b) Y_{H_2O} , (c) Y_{CO_2} , (d) Y_{H_2} at $x/d = 30$ in flame E compared with flamelet calculations with and without the unity Lewis number assumption.

experimentally is affected by statistical uncertainty. Thus, for the present study it is more effective to use flamelet solutions than conditional means.

3.1. The conditionally filtered diffusion of mixture fraction and temperature perturbations

The conditionally filtered diffusion of the flamelet temperature and that of the temperature perturbations at $x/d = 30$ in flame E, $\langle \langle \frac{1}{\rho} \frac{\partial}{\partial y} (\rho D \frac{\partial T^f}{\partial y}) | Z, T \rangle_\ell | \langle Z \rangle_L, \langle Z'^2 \rangle_L \rangle$ and $\langle \langle \frac{1}{\rho} \frac{\partial}{\partial y} (\rho D \frac{\partial T^*}{\partial y}) | Z, T \rangle_\ell | \langle Z \rangle_L, \langle Z'^2 \rangle_L \rangle$ respectively, are shown in Fig. 2 along with the mixture fraction diffusion. Because they are transport velocities of the FMDF in the mixture fraction-temperature sample space, we present them as a diffusion velocity in the form of streamlines and magnitudes [23,24]. Here the mixture fraction diffusion is non-dimensionalized by the square root of the SGS variance $\langle Z'^2 \rangle_L^{1/2}$ and the Favre conditional scalar dissipation rate, $\langle \langle \chi \rangle_L | \langle Z \rangle_L, \langle Z'^2 \rangle_L \rangle$ while the temperature diffusion is non-dimensionalized using the peak temperature and the Favre conditional temperature dissipation, $\langle \langle \chi_T \rangle_L | \langle Z \rangle_L, \langle Z'^2 \rangle_L \rangle$. Since $T^f = T^f(Z, \chi_s^f)$, the diffusion of T^f depends on the mixture fraction, the scalar dissipation and diffusion as follows:

$$\begin{aligned} & \left\langle \frac{1}{\rho} \frac{\partial}{\partial y} \left(\rho D \frac{\partial T^f}{\partial y} \right) \middle| Z, T \right\rangle_\ell \\ &= \frac{\partial T^f}{\partial Z} \left\langle \frac{1}{\rho} \frac{\partial}{\partial y} \left(\rho D \frac{\partial Z}{\partial y} \right) \middle| Z, T \right\rangle_\ell + \frac{\partial^2 T^f}{\partial Z^2} \left\langle D \frac{\partial Z}{\partial y} \frac{\partial Z}{\partial y} \middle| Z, T \right\rangle_\ell. \end{aligned} \quad (6)$$

Near the peak temperature the mixture fraction diffusion is small because this region is close to the center of the ramp-cliff structure. The diffusion of T^f is negative due to the negative curvature of the T^f profiles as a function of mixture fraction (Fig. 2b). Consequently, the streamlines starting near the peak temperature nearly move

vertically toward lower temperatures. As the streamlines move toward lower temperatures, the scalar dissipation increases, resulting in larger diffusion magnitudes. For very lean and rich mixtures, the dominant term for the diffusion of T^f is the first term on the RHS of Eq. (6) so that the diffusion of T^f is proportional to mixture fraction diffusion, which results in long straight streamlines along the direction of ridgeline of the FMDF [25]. This diffusion streamline pattern is very similar to that of the conditionally filtered diffusion of T (Fig. 2a) [25], suggesting that the steady flamelet can represent much of the coupling between mixing and reaction. The pattern is, however, very different from that of non-reacting scalar mixing [23], which tends to have streamlines converting to the conditional mean, further highlighting the effects of reaction in inducing diffusion.

Figure 2 c and d shows the conditionally filtered diffusion of Z and T^* plotted in the $Z - T$ and $Z - T^*$ sample space, respectively. Unlike those in Fig. 2b, the diffusion velocity streamlines generally move first toward a manifold close to T^f , which is also close to the ridgeline of the FMDF [23]. The diffusion velocity magnitude decreases as it approaches T^f . The streamlines then move along the manifold at lower velocities. In addition, the magnitude of the diffusion velocity is generally smaller than that of T [23]. Figure 2d further shows that the streamlines largely move toward $T^* = 0$ near the peak temperature, i.e., the dominant effect of diffusion is to reduce T^* . This SGS mixing pattern of the mixture fraction and the temperature perturbations is similar to that of three (non-reactive) scalar mixing in a turbulent coaxial jet [26] and to the temperature mixing in distributed reaction zones [23]. The coaxial jet consists of a center jet, an annular flow, and a co-flow. The spatial relationship among the scalars carried by each stream is similar to the fuel-product-oxidizer relationship in a non-premixed reaction flow. However, the pattern is qualitatively different from the conditionally filtered diffusion of T^f , for which the streamlines move toward lower temperature, not the conditional mean temperature. The diffusion results for Y_{H_2O} is also similar (not shown).

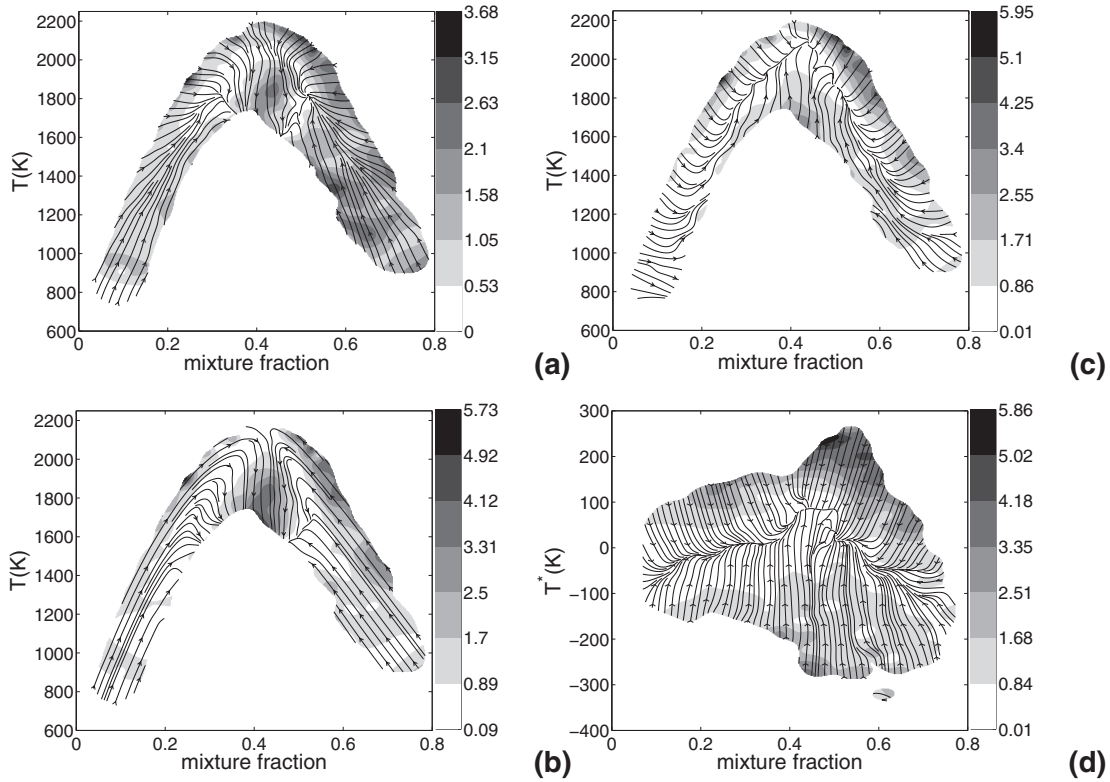


Fig. 2. (a) Conditionally filtered mixture fraction diffusion and temperature diffusion; (b) the flamelet part; (c) conditionally filtered mixture fraction diffusion and temperature perturbation diffusion conditional on temperature and (d) conditionally filtered mixture fraction diffusion and temperature perturbation diffusion conditional on temperature perturbation. All figures are for flame E at $x/d = 30$. The gray scales denote the magnitude of the diffusion velocity vector.

The similarities between the form of the conditionally filtered diffusion of T^* and that of a non-reactive scalar suggest that the former may be modeled using the Interaction by Exchange with the Mean (IEM) model [27], which was developed based on non-reactive scalar mixing characteristics. The IEM model for the conditionally filtered temperature perturbation diffusion is

$$\left\langle \frac{1}{\rho} \frac{\partial}{\partial x_i} \left(\rho D \frac{\partial T^*}{\partial x_i} \right) \middle| Z, T^* \right\rangle_\ell = -\frac{T^*}{2\tau_{T^*}}, \quad (7)$$

where τ_{T^*} is the mixing time scale for T^* . To examine the trend of the diffusion more clearly in Fig. 3 we plot the conditionally filtered diffusion of T^* as a function of T^* at $x/d = 15$ and 30 in flames D and E. The overall linear trend is indeed consistent with the IEM model. Note that the IEM model is qualitatively inconsistent with the diffusion of T^f , which is not toward the conditional mean temperature due to the coupling of the diffusion to the reaction. The issue of the choice τ_{T^*} and the comparison between the experiment results and the IEM model will be discussed in Section 3.3.

Two other commonly used mixing models are the Modified Curl (MC) model and the Euclid Minimum Spanning Tree (EMST) model. These models are stochastic models, thus their performance cannot be directly evaluated from experimental data. Nevertheless, we expect that their performance will be improved if only the diffusion of the perturbations from flamelets is modeled, although may be to a lesser extent than the IEM model. For example, since mixing in the MC model occurs between pairs of stochastic particles, if two particles lie on a flamelet but have different mixture fraction values, the mixed particle will not be on the flamelet due to the curvature of the $T-Z$ curve, which is inconsistent with the flamelet solution. However, if only mixing of the perturbations from the flamelet is modeled, the mixed particle will still be on the flamelet. The EMST model is local in composition space, its performance will probably not be strongly affected by modeling diffusion of the perturbations. Never-

theless, we still expect some improvement of its performance since the non-localness is reduced for the perturbations. However, the extent of improvement will perhaps be the smallest among the three models discussed.

3.2. The conditional filtered dissipation rate for temperature perturbations

The conditionally filtered dissipation rate of the flamelet part and its perturbations filtered conditionally on both the mixture fraction and temperature, $\langle \langle 2D \frac{\partial T^f}{\partial y} \frac{\partial T^f}{\partial y} | Z, T \rangle_\ell | \langle Z \rangle_L, \langle Z'^2 \rangle_L \rangle$ and $\langle \langle 2D \frac{\partial T^*}{\partial y} \frac{\partial T^*}{\partial y} | Z, T \rangle_\ell | \langle Z \rangle_L, \langle Z'^2 \rangle_L \rangle$ are shown in Fig. 4. The cross-dissipation term is generally small compared to the other two terms and is not shown. For the flamelet part, its dissipation only depends on the scalar and the scalar dissipation rate:

$$\chi_{T^f} \equiv \left\langle 2D \frac{\partial T^f}{\partial y} \frac{\partial T^f}{\partial y} \middle| Z, T \right\rangle_\ell = \left(\frac{\partial T^f}{\partial Z} \right)^2 \left\langle 2D \frac{\partial Z}{\partial y} \frac{\partial Z}{\partial y} \middle| Z, T \right\rangle_\ell. \quad (8)$$

The conditionally filtered temperature dissipation rate of the flamelet part has two peak values, one on the lean side near $Z = 0.3$ and one on the rich side near $Z = 0.5$ and (Fig. 4b), where the conditionally filtered scalar dissipation rate is generally large at lower temperatures [25]. Near the peak temperature $\frac{\partial T^f}{\partial Z}$ is approximately zero, which results in a lower dissipation rate of T^f . Because the tight coupling between T^f and Z , χ_{T^f} can be obtained from the conditionally filtered scalar dissipation rate.

Figure 4 c shows the conditionally filtered dissipation rate of T^* . Unlike $\langle \chi_{T^f} | Z, T \rangle_\ell$ (Fig. 4b) and $\langle \chi_T | Z, T \rangle_\ell$ (Fig. 4a), there is generally one peak near $Z = 0.45$ at a lower temperature where the maximum gradient in the ramp-cliff structure is located. Thus, the dependence of $\langle \chi_{T^*} | Z, T \rangle_\ell$ on T and Z has some similarities to that of a nonreactive scalar and temperature in distributed reaction zones [25]. Compared

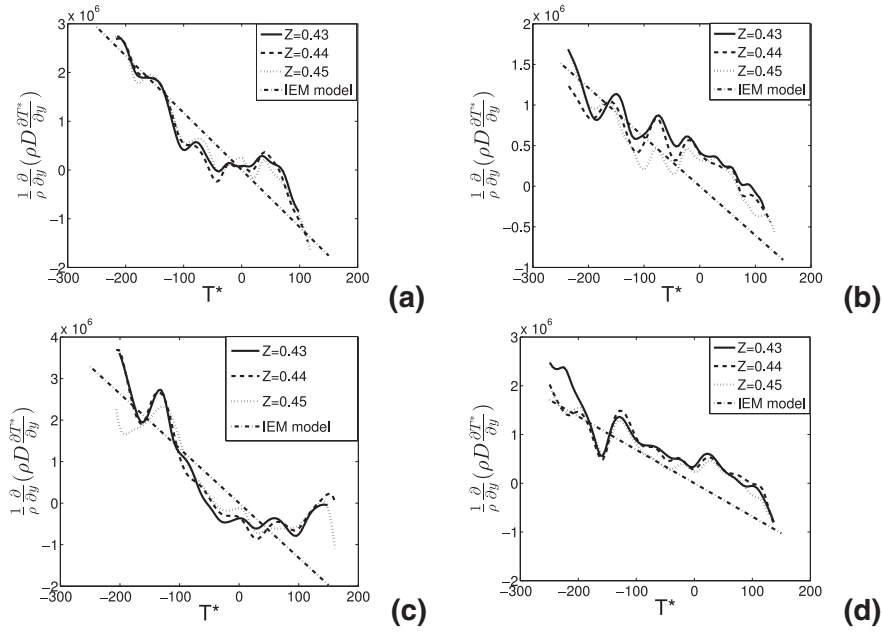


Fig. 3. Conditionally filtered temperature perturbation diffusion near the peak temperature in flame E compared with the mixing time scale given in Eq. (30) and a C value of 2.5. The unit for the diffusion is K^2/s . (a) At $x/d = 15$ in flame D, $\chi_s = 245.8/\text{s}$; (b) $x/d = 30$ in flame D, $\chi_s = 126.8/\text{s}$; (c) $x/d = 15$ in flame E, $\chi_s = 275.8/\text{s}$; (d) $x/d = 30$ in flame E, $\chi_s = 143.5/\text{s}$.

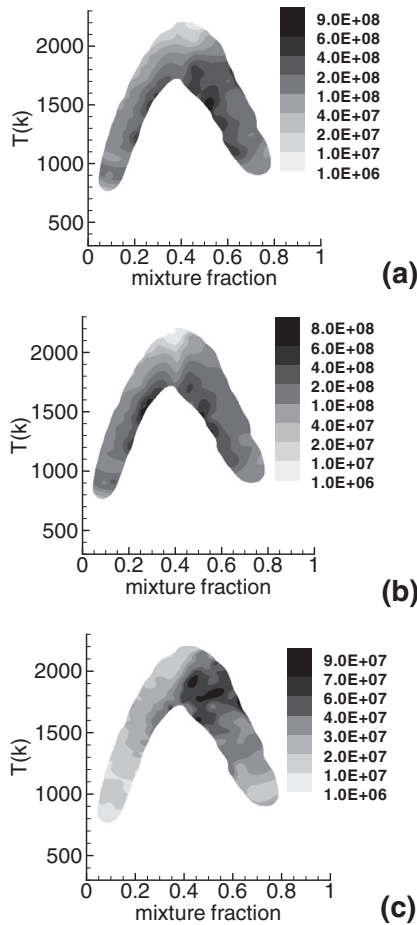


Fig. 4. Conditionally filtered dissipation rate of (a) T and (b) T' and (c) T^* at $x/d = 30$ in flame E. The unit for the dissipation is K^2/s .

to Fig. 4b, the dissipation rate of T^* is almost an order of magnitude smaller than that of T' , indicating that the dominant contributions of the conditionally filtered temperature dissipation rate come from the flamelet structure and that the mixing of T^* may pose a lesser modeling challenge.

3.3. Asymptotic analysis of the perturbations from flamelets

The similar functional forms of SGS diffusion and dissipation of reactive scalar perturbations observed in Sections 3.1 and 3.2 to those of a non-reactive scalar suggest that they may be modeled in a similar way. To further understand the reactive scalar perturbations, such as their dynamics and time and length scales, we perform perturbation analysis of the flamelet equation. We will consider two possible limiting forms of the perturbations, whose length scales are small and large compared to the reaction zone width, respectively. While these forms only represent the perturbations in flames under limiting conditions, they nevertheless can help us understand the nature and behaviors of the perturbations. Consistent with our objective of examining mixing in burning flamelets and perturbations from them, in the analysis we assume that χ_s^f is far from the extinction limit (high Damköhler number).

Starting from the transport equation for reactive scalars ϕ_i ,

$$\rho \frac{\partial \phi_i}{\partial t} + \rho u_k \frac{\partial \phi_i}{\partial x_k} - \frac{\partial}{\partial x_k} \left(\rho D \frac{\partial \phi_i}{\partial x_k} \right) = w_i, \quad (9)$$

with the coordinate transformation using $Z_2 = x_2$, $Z_3 = x_3$, $t^* = t$, and replacing the coordinate x_1 by Z , we obtain

$$\begin{aligned} \frac{\partial}{\partial t} &= \frac{\partial}{\partial t^*} + \frac{\partial Z}{\partial t} \frac{\partial}{\partial Z}, & \frac{\partial}{\partial x_1} &= \frac{\partial Z}{\partial x_1} \frac{\partial}{\partial Z} \\ \frac{\partial}{\partial x_k} &= \frac{\partial}{\partial Z_k} + \frac{\partial Z}{\partial x_k} \frac{\partial}{\partial Z}, & (k=2,3) \end{aligned} \quad (10)$$

one obtains the flamelet equation [28]

$$\rho \frac{\partial \phi_i}{\partial t^*} = \rho D \nabla Z \cdot \nabla Z \frac{\partial^2 \phi_i}{\partial Z^2} + w_i + R, \quad (11)$$

where

$$R = -\rho \left(u_2 \frac{\partial \phi_i}{\partial Z_2} + u_3 \frac{\partial \phi_i}{\partial Z_3} \right) + \frac{\partial(\rho D)}{\partial x_2} \frac{\partial \phi_i}{\partial Z_2} - \frac{\partial(\rho D)}{\partial x_3} \frac{\partial \phi_i}{\partial Z_3} + \rho D \left[\left(\frac{\partial Z}{\partial x_k} \right)^2 \frac{\partial^2 \phi_i}{\partial Z^2} + 2 \frac{\partial Z}{\partial x_2} \frac{\partial^2 \phi_i}{\partial Z \partial Z_2} + 2 \frac{\partial Z}{\partial x_3} \frac{\partial^2 \phi_i}{\partial Z \partial Z_3} + \frac{\partial^2 \phi_i}{\partial Z_2^2} + \frac{\partial^2 \phi_i}{\partial Z_3^2} \right]. \quad (12)$$

To perform singular perturbation expansions with the inner layer containing the stoichiometric mixture fraction, stretched coordinates are introduced

$$\zeta = \frac{Z - Z_s}{\epsilon}, \quad \tau = \frac{t^*}{\epsilon^2}, \quad (13)$$

the reactive scalars and the reaction rate are then expanded into leading-order and first-order terms

$$\nabla \phi_i = \nabla \phi_i^0 + \epsilon \nabla \phi_i^1, \quad (14)$$

$$w_i = w_i^0 + \left(\frac{\partial w_i}{\partial \phi_j} \right)^0 \epsilon \phi_j^1, \quad (15)$$

where a superscript denotes the order. Since perturbations from flamelets are caused by perturbations in the mixture fraction gradient, we expand the latter as

$$\nabla Z = \nabla Z^0 + \epsilon \nabla Z^1. \quad (16)$$

Substituting Eqs. (13)–(16) into the flamelet equation and using the mixture fraction transport equation,

$$\rho \frac{\partial Z}{\partial t} + \rho u_k \frac{\partial Z}{\partial x_k} - \frac{\partial}{\partial x_k} \left(\rho D \frac{\partial Z}{\partial x_k} \right) = 0, \quad (17)$$

we obtain the leading-order equation

$$\rho \frac{\partial \phi_i^0}{\partial \tau} = \rho \frac{\chi^0}{2} \frac{\partial^2 \phi_i^0}{\partial \zeta^2} + \epsilon^2 w_i^0, \quad (18)$$

and the equation for the first-order perturbation

$$\begin{aligned} \rho \frac{\partial \phi_i^1}{\partial \tau} &= \rho \frac{\chi^0}{2} \frac{\partial^2 \phi_i^1}{\partial \zeta^2} + \rho \frac{\chi^1}{2} \frac{\partial^2 \phi_i^0}{\partial \zeta^2} + \epsilon^2 \left(\frac{\partial w_i}{\partial \phi_j} \right)^0 \phi_j^1 \\ &\quad - \rho D \sum_{k=2}^3 2 \frac{\partial Z^0}{\partial x_k} \frac{\partial^2 (\phi_i^0 + \epsilon \phi_i^1)}{\partial \zeta \partial Z_k} \\ &= \rho \frac{\chi^0}{2} \frac{\partial^2 \phi_i^1}{\partial \zeta^2} + \rho \frac{\chi^1}{2} \frac{\partial^2 \phi_i^0}{\partial \zeta^2} + \epsilon^2 \left(\frac{\partial w_i}{\partial \phi_j} \right)^0 \phi_j^1 \\ &\quad - \epsilon \rho D \sum_{k=2}^3 2 \frac{\partial Z^0}{\partial x_k} \frac{\partial^2 \phi_i^1}{\partial \zeta \partial Z_k}, \end{aligned} \quad (19)$$

where $\chi^0 = 2D\nabla Z^0 \cdot \nabla Z^0$ and $\chi^1 = 4D\nabla Z^0 \cdot \nabla Z^1$ are the flamelet dissipation rate and the dissipation perturbation, respectively. The terms on the RHS of Eq. (19) are the diffusion of the perturbation, production of the perturbation due to the scalar dissipation rate perturbation, the reaction source term, and the curvature term, respectively. The curvature term containing ϕ_i^0 vanishes because there are no curvature effects in the (leading-order) equation for ϕ_i^0 . The perturbation ∇Z^1 must be of order one in order for ϕ_i^1 to be of the same order: $\epsilon \nabla Z^1 \sim \nabla Z^0 \frac{\ell_R}{\ell} \sim \epsilon \nabla Z^0$, where ℓ and ℓ_R are the length scale of ∇Z^0 and the reaction zone width, respectively. We further decompose ∇Z^1 and χ^1 into $\nabla Z^1 = \nabla Z^{1f} + \nabla Z^{1*}$ and $\chi^1 = \chi^{1f} + \chi^{1*}$, where ∇Z^{1f} , χ^{1f} , ∇Z^{1*} , and χ^{1*} represent the slow variations of ∇Z and χ (or the first-order corrections to ∇Z^0 and χ^0 , respectively) inside the reaction zone and the perturbations from the flamelet ($\nabla Z^0 + \epsilon \nabla Z^1$,

$\chi^0 + \chi^1$), respectively. Correspondingly, ϕ_i^{1f} and ϕ_i^{1*} are the first-order correction to ϕ_i^0 and the perturbations resulting from χ^{1*} , respectively. In the following we consider two limiting cases of χ^{1*} with its length scales, ℓ_1 , much smaller and larger than the reaction zone width respectively.

1. Perturbations with $\ell_1 \ll \ell_R$

For the case $\ell_1 \ll \ell_R$, the perturbations could potentially result in a greater curvature of the mixing fraction field. However, the curvature of the perturbed mixture fraction field ($Z = Z^0 + \epsilon(Z^{1f} + Z^{1*})$) must remain of order ϵ for the leading-order expansion to be valid. The curvature without the fluctuations ∇Z^{1*} is $\frac{\ell_R}{\ell} \sim \epsilon$. When ∇Z^{1*} has fluctuations of scale $\ell_1 \ll \ell_R$ the curvature is

$$\frac{\epsilon(|\nabla Z^{1*}|/|\nabla Z^0|)\ell_1}{\ell_1} = \epsilon \frac{|\nabla Z^{1*}|}{|\nabla Z^0|}, \quad (20)$$

where $\epsilon|\nabla Z^{1*}| \ell_1$ is the change of scalar difference over the length ℓ_1 due to ∇Z^{1*} ; therefore $\epsilon(|\nabla Z^{1*}|/|\nabla Z^0|)\ell_1$ is the displacement of the iso-mixture fraction contour. If ∇Z^{1*} is of order one or less, the curvature induced by ∇Z^{1*} is of the same order to or smaller than the curvature of the Z^0 field, i.e., $\frac{|\nabla Z^{1*}|}{|\nabla Z^0|} \leq \epsilon$. Thus, for $|\nabla Z^{1*}| \ll |\nabla Z^0|$, i.e., for a perturbation gradient much smaller than the flamelet gradient, the flamelet structure is preserved, even when scalar fluctuations are present in the reaction zone.

For isotropic ∇Z^1 perturbations, the orders of magnitude of the diffusion term and the curvature term in Eq. (19) can be estimated as

$$\rho \frac{\chi^0}{2} \frac{\phi_i^{1*}}{\ell_1^2 \nabla Z^0 \cdot \nabla Z^0 / \epsilon^2} = \epsilon^2 \rho D \frac{\phi_i^{1*}}{\ell_1^2} \quad (21)$$

and

$$\epsilon \rho D \nabla Z^0 \frac{\phi_i^{1*}}{\ell_1 \nabla Z^0 \ell_1 / \epsilon} = \epsilon^2 \rho D \frac{\phi_i^{1*}}{\ell_1^2}, \quad (22)$$

respectively. Thus, the two terms are of the same order of magnitude. The reaction term, on the other hand, is smaller, as will be shown below.

For $\ell_1 \ll \ell_R$, the variables χ^0 , $\frac{\partial^2 \phi_i^0}{\partial \zeta^2}$, and $\frac{\partial Z^0}{\partial x_k}$ in Eq. (19) can be considered as independent of ζ . Fourier transform the first order equation, we have

$$\begin{aligned} \rho i \omega \widehat{A}_i &= -\rho \frac{\chi^0}{2} \widehat{A}_i k_\zeta^2 + \frac{1}{2} \rho \frac{\partial^2 \phi_i^0}{\partial \zeta^2} \widehat{\chi}^{1*} + \epsilon^2 \left(\frac{\partial w_i}{\partial \phi_j} \right)^0 \widehat{A}_j \\ &\quad + \rho D \sum_{m=2}^3 \frac{\partial Z^0}{\partial x_m} \epsilon \widehat{A}_i k_\zeta k_m \end{aligned} \quad (23)$$

$$\begin{aligned} \left[\rho i \omega \delta_{ij} + \rho \frac{\chi^0}{2} k_\zeta^2 \delta_{ij} - \epsilon^2 \left(\frac{\partial w_i}{\partial \phi_j} \right)^0 - \epsilon \rho D \sum_{m=2}^3 \frac{\partial Z^0}{\partial x_m} (k_\zeta k_m) \right] \widehat{A}_i \\ = \frac{1}{2} \rho \frac{\partial^2 \phi_i^0}{\partial \zeta^2} \widehat{\chi}^{1*} \end{aligned} \quad (24)$$

where $\widehat{A}_i = \widehat{A}_i(\omega, k_\zeta, k_2, k_3)$ and $\widehat{\chi}^{1*} = \widehat{\chi}^{1*}(\omega, k_\zeta, k_2, k_3)$ are the Fourier transforms of ϕ_i^{1*} and χ^{1*} respectively, and ω , k_ζ , k_2 , k_3 are the angular frequency, wavenumber in the ζ direction, and wavenumber in the x_2 and x_3 directions, respectively. An overbar denotes the spatially averaged value in the reaction zone. The terms in the bracket on the LHS can be inverted to obtain the transfer function of the system described by Eq. (24) which is a frequency-wavenumber filter of first and second orders, respectively, acting on the production (or forcing) term $\frac{1}{2} \rho \frac{\partial^2 \phi_i^0}{\partial \zeta^2} \widehat{\chi}^{1*}$. The reaction term does not depend on the wavenumber, and consequently is small compared to the second term (diffusion) for small-scale perturbations, because

for $k_\zeta > \frac{\epsilon}{\Delta Z_R}$,

$$\frac{\chi^0}{2} k_\zeta^2 > \frac{\chi^0}{2} \frac{\epsilon^2}{(\Delta Z_R)^2} \approx \epsilon^2 \frac{\chi^0}{2} \frac{\phi^0}{Z_s(1-Z_s)\Delta Z_R} \frac{Z_s(1-Z_s)}{\Delta Z_R \phi^0}$$

$$\approx \rho \frac{\chi^0}{2} \frac{\partial^2 \phi^0}{\partial \zeta^2} \frac{Z_s(1-Z_s)}{\phi^0 \Delta Z_R} \tag{25}$$

$$\approx \epsilon^2 w^0 \frac{Z_s(1-Z_s)}{\phi^0 \Delta Z_R} \approx \epsilon^2 \left(\frac{\partial w}{\partial \phi} \right)^0 \frac{Z_s(1-Z_s)}{\Delta Z_R} \approx \epsilon^2 \left(\frac{\partial w}{\partial \phi} \right)^0, \tag{26}$$

i.e., the reaction term does not significantly alter the filter function at high wavenumbers. The perturbation ϕ_i^{1*} is essentially proportional to the filtered production term, with the filter function largely determined by the mixture fraction field, and the length scale determined by ∇Z^1 . Therefore, it is expected to have diffusion characteristics that are similar to a non-reactive scalar, such as the functional form of the conditionally filtered diffusion and the SGS mixing time scale. Physically, when the perturbations occur at high wavenumbers ($k \sim 1/\ell_1 \gg 1/\ell_R$), their dynamics are dominated by the forcing term and the diffusion term. This type of perturbations are likely to occur in high-Reynolds number flames where the dissipation length scales are smaller than the reaction zone width.

2. Perturbations with $\ell_1 \gg \ell_R$

For $\ell_1 \gg \ell_R$, χ^{1*} is independent of ζ in the reaction zone, and is only a function of time. Thus the perturbations essentially cause type the flamelet to become unsteady or quasi-steady. For isotropic ∇Z^1 perturbations, the orders of magnitude of the diffusion term and the curvature term in Eq. (19) can be estimated as

$$\rho \frac{\chi^0}{2} \frac{\phi_i^{1*}}{\ell_R^2 \nabla Z^0 \cdot \nabla Z^0 / \epsilon^2} = \epsilon^2 \rho D \frac{\phi_i^{1*}}{\ell_R^2} \tag{27}$$

and

$$\epsilon \rho D \nabla Z^0 \frac{\phi_i^{1*}}{\ell_R \nabla Z^0 \ell_1 / \epsilon} = \epsilon^2 \rho D \frac{\phi_i^{1*}}{\ell_R \ell_1}, \tag{28}$$

respectively. The curvature term therefore is much smaller and is neglected in the following analysis.

The Fourier transform of Eq. (19) is

$$\rho i \omega \widehat{A}(k, \omega) = -\rho \frac{\chi^0}{2} \widehat{A} k_\zeta^2 + \frac{1}{2} \rho \frac{\partial^2 \widehat{\phi}^0}{\partial \zeta^2} \widehat{\chi}^{1*}(\omega) + \epsilon^2 \left(\frac{\partial w_i}{\partial \phi_j} \right)^0 * \widehat{A}_j. \tag{29}$$

The spatial variations of ϕ_i^{1*} is now determined by $\frac{\partial^2 \phi^0}{\partial \zeta^2}$ and $\left(\frac{\partial w_i}{\partial \phi_j} \right)^0$. Since both terms are limited to the reaction zone, so is the diffusion term. Thus, the length scales of these terms are of the order of the reaction width. The orders of magnitudes of the diffusion and reaction terms are estimated as $\rho \frac{\chi^0}{2} \phi_i^{1*}$ and $\epsilon^2 \frac{w_i^0 \phi_j^{1*}}{\phi_j^0}$, respectively, and therefore, are of the same order. This shows that the diffusion is strongly influenced by reaction. The temporal variations of ϕ_i^{1*} is largely determined by χ^{1*} through a first-order filter.

The diffusion term in Eq. (19) is largely limited to the reaction zone, and therefore can be estimated as $\rho \frac{\chi^0}{2} \frac{\partial^2 \phi_i^{1*}}{\partial Z^2} \sim -\rho \frac{\chi^0}{2} \frac{\phi_i^{1*}}{Z_s(1-Z_s)\Delta Z_R}$, which can be expressed in the same form as the IEM model:

$$-C \frac{\chi^0}{2} \frac{\phi_i^{1*}}{Z_s(1-Z_s)\Delta Z_R} = -C \frac{\phi_i^{1*}}{2\tau_{\phi_i^{1*}}}, \tag{30}$$

where $\tau_{\phi_i^{1*}} = \frac{Z_s(1-Z_s)\Delta Z_R}{\chi^0}$ and C is the SGS mixing time for ϕ_i^{1*} and the model coefficient respectively. Since the estimate should also be valid for nearly steady flamelet, we show in Fig. 5 the perturbation

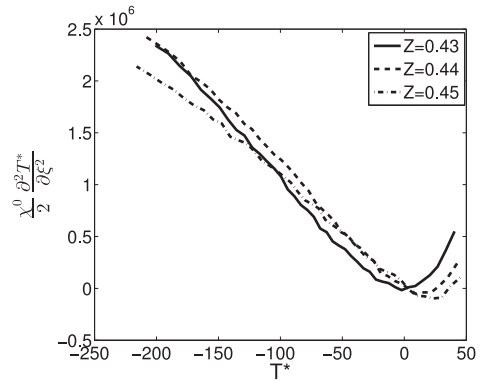


Fig. 5. Conditionally filtered temperature perturbation diffusion near the peak temperature from flamelet solutions with $\chi_s^f = 143/s$.

diffusion from the steady flamelet (differences between the dominant flamelet and other flamelets) near the peak temperature. The overall functional form is indeed consistent with the IEM model. Thus, while the diffusion of T^f has qualitatively different characteristics than that of a non-reactive scalar, the perturbation diffusion has similarities to the latter.

The above asymptotic analysis suggests that the diffusion of the reactive scalar perturbations, whether in the form of small-scale random fluctuations or unsteady flamelets, has the form of non-reactive scalars, but with different mixing times. To examine which forms of the perturbations are more consistent with those observed in the Sandia flames, in Fig. 3 we compare the experimental results of the conditionally filtered diffusion of T^f ($= \epsilon T^{1*}$) near the peak temperature to the prediction of the IEM model using $\tau_T^* = \tau_{\phi_i^{1*}}$ (Eq. (30)). The results at $x/d = 15$ and 30 in flames D and E cover two Reynolds numbers, two SGS variance values (the SGS variance values at the same downstream locations are approximately equal for the two flames), and four scalar dissipation rate values, and therefore are good test cases for the scaling of the mixing time scale. The approximately linear trend of the experimental results is consistent with the IEM model. Perhaps more important, the magnitude of the measured diffusion is consistent with the IEM model having the mixing time given by Eq. (30) and a C value of 2.5 for all the cases. The significance of these results is that the mixing time appears to scale with $\tau_{\phi_i^{1*}}$. Using the time scale of SGS mixture fraction, on the other hand, would require different C values for the model to fit the data for the different cases. The overall similarity of the experimental results to the flamelet solutions suggests that the perturbation diffusion is consistent with predictions based on unsteady or quasi-steady flamelets.

4. Discussions and conclusions

In the present work we used data obtained in turbulent partially premixed flames (Sandia flames) to study SGS mixing of temperature perturbations from steady flamelets. The Favre filtered mixture fraction and Favre filtered SGS scalar variance were used as conditioning variables for analyzing the conditionally filtered dissipation and diffusion of temperature perturbations. We focus on the temperature and Y_{H_2O} in flame E at $x/d = 30$ where the Reynolds number is high and the differential diffusion effects for these variables are negligible. We chose the flamelet with $T^f(Z, \chi_s^f)$ closest to the conditionally filtered temperature $\langle \langle T|Z \rangle_L | \langle Z \rangle_L, \langle Z'^2 \rangle_L$ for the burning samples. Due to the limited amount of data available, we obtained results for one large SGS variance value. If other values are chosen, the dissipation rate χ_s for flamelets that match the conditional mean values will vary. Since $\langle Z'^2 \rangle_L$ is a fluctuating quantity in a turbulent flame, so does χ_s , allowing the analysis to account for the scalar dissipation rate fluctuations.

The results show that for large SGS variance, the streamline representing the conditionally filtered diffusion of mixture fraction and temperature perturbations for the nearly fully burning samples generally converge quickly to a manifold close to $T^f(Z, \chi_s^f)$, along which they continue at lower velocities, i.e., the dominant effect of the diffusion is to reduce T^* . The conditionally filtered dissipation rate of the temperature perturbations is generally much smaller than the value from the flamelet part. The peak value is near $\xi = 0.4\text{--}0.45$ at lower temperature where the maximum gradient in the ramp-cliff structure is located. These mixing patterns are very similar to those of three non-reactive scalar mixings in a turbulent coaxial jet. Further analysis shows that the functional form of the diffusion is well described by the IEM model.

Our perturbation analysis of the flamelet equation shows that for perturbations having length scales smaller than the reaction zone width, the reactive scalar diffusions are largely controlled by the mixture fraction field, thus having the characteristics of non-reactive scalar mixing. This type of perturbations probably requires high Reynolds numbers so that the scalar dissipation length scale is smaller than the reaction zone width. For perturbations with length scales larger than the reaction width, which are consistent with unsteady or quasi-steady flamelets, the conditionally filtered diffusion has the same form as non-reactive scalar mixing, with the mixing time scale depending on Z_s and ΔZ_R . The IEM model predictions based on this mixing time scale are in good agreement with the experimental results for a range of SGS conditions, suggesting that the perturbations for the conditions studied are consistent with unsteady or quasi-steady flamelets.

The present study suggests that mixing models that are based on non-reactive scalars can potentially model the mixing of the reactive scalar perturbations from flamelets accurately. Because the mixing models do not need to model the flamelet part, the total reactive scalar diffusion (the flamelet part plus the perturbations) can be modeled more accurately. Since most current mixing models already perform well for distributed reaction zones, the results in the present study can be useful for developing a unified mixing model that can predict all combustion regimes, including distributed reaction zones and flamelets accurately.

Acknowledgments

We thank Dr. Robert Barlow and Professor Adonios Karpetsis for providing the Sandia flame data and Professor Heinz Pitsch for providing the software FlameMaster. This work was supported by the National Science Foundation under grant no. CBET-1333489.

References

- [1] S.B. Pope, *Proc. Combust. Inst.* 34 (2013) 1–31.
- [2] D.C. Haworth, M.C. Drake, S.B. Pope, *Proc. Combust. Inst.* 22 (1988) 589–597.
- [3] S.B. Pope, *Annu. Rev. Fluid Mech.* 19 (1987) 237–270.
- [4] R.W. Bilger, *Combust. Sci. Tech.* 22 (1980) 251–261.
- [5] N. Peters, *Turbulent Combustion*, Cambridge University Press, Cambridge, England, 2000.
- [6] S.B. Pope, *Prog. Energy Combust. Sci.* 11 (1985) 119–192.
- [7] C. Tong, *Phys. Fluids* 13 (2001) 2923–2937.
- [8] A.G. Rajagopalan, C. Tong, *Phys. Fluids* 15 (2003) 227–244.
- [9] D. Wang, C. Tong, *Phys. Fluids* 14 (2002) 2170–2185.
- [10] D. Wang, C. Tong, S.B. Pope, *Phys. Fluids* 16 (2004) 3599–3613.
- [11] D. Wang, C. Tong, *Proc. Combust. Inst.* 30 (2005) 567–574.
- [12] D. Wang, C. Tong, R.S. Barlow, A.N. Karpetsis, *Proc. Combust. Inst.* 31 (2007) 1533–1541.
- [13] A.N. Karpetsis, R.S. Barlow, *Proc. Combust. Inst.* 29 (2002) 1929–1936.
- [14] A.N. Karpetsis, R.S. Barlow, *Proc. Combust. Inst.* 30 (2005) 665–672.
- [15] R.S. Barlow, A.N. Karpetsis, *Flow, Turb. Combust.* 72 (2004) 427–448.
- [16] H. Pitsch, FlameMaster v3.31, A C++ Computer Program for OD Combustion and 1D Laminar Flame Calculations.
- [17] G.P. Smith, D.M. Golden, M. Frenklach, N.W. Moriarty, B. Eiteneer, M. Goldenberg, C.T. Bowman, R.K. Hanson, S. Song, W.C. Gardiner, J.V.V. Lissianski, Z. Qin, http://www.me.berkeley.edu/gri_mech/.
- [18] R.S. Barlow, J.H. Frank, A.N. Karpetsis, J.-Y. Chen, *Combust. Flame* 143 (2005) 433–449.
- [19] R.S. Barlow, A.N. Karpetsis, J.H. Frank, J.-Y. Chen, *Combust. Flame* 127 (2001) 2102–2118.
- [20] J.H. Frank, R.S. Barlow, C. Lundquist, *Proc. Combust. Inst.* 28 (2000) 447–454.
- [21] A. Wang, M.F. Modest, D.C. Haworth, L. Wang, *JQSRT* 109 (2008) 269–279.
- [22] G. Wang, A.N. Karpetsis, R.S. Barlow, *Combust. Flame* 148 (2007) 62–75.
- [23] J. Cai, R.S. Barlow, A.N. Karpetsis, C. Tong, *Proc. Combust. Inst.* 33 (2011) 1505–1513.
- [24] S.S. Liu, C. Tong, *Proc. Combust. Inst.* 34 (2013) 1231–1239.
- [25] J. Cai, D. Wang, C. Tong, R.S. Barlow, A.N. Karpetsis, *Proc. Combust. Inst.* 32 (2009) 1517–1525.
- [26] J. Cai, M.J. Dinger, C.D. Carter, M.D. Ryan, C. Tong, *J. Fluid Mech.* 685 (2011) 495–531.
- [27] J. Villiermaux, J.C. Devillon, *Proceedings of Second International Symposium on Chemical Reaction Engineering* (1972) 1–13.
- [28] N. Peters, *Prog. Eng. Combust. Sci.* 10 (1984) 319–339.